An investigation of adiabatic spiral vortex flow by means of cross-wire probes

C. C. Wan* and J. E. R. Coney†

Flow transitions occurring with increase in the Taylor number in an annular gap of radius ratio 0.8, having an imposed axial flow of air of Reynolds number 500, have been studied using the output from a cross-wire probe in a complex digital analysis. Cross and phase spectra, together with auto and cross correlograms, are presented for four Taylor numbers from 10 620 to 12.2×10^6, covering the onset of vortex flow, chaotic flow and turbulent vortex flow. As the Taylor number increases, there is little alteration in the spiral vortex flow in the axial and tangential directions, which oscillates in phase in these two directions. The tangential velocity gradient was seen to become increasingly dominant, with increase in the Taylor number

Key words: *turbulent flow, vortices, flow transitions*

Investigations into the stability of the flow in an annular gap, using a combination of hot-wire anemometry and digital techniques, were described in a recent paper[1]. With the annular gap comprised of a stationary outer cylinder and a rotating inner cylinder and with an imposed axial flow of the working fluid (air) through the gap, various transition modes were observed. After the onset of spiral vortex flow, the well-known wavy mode was detected. Thereafter and prior to a breakdown into turbulence, a form of instability was encountered, which was termed chaotic. In this study a cross-wire probe was used to investigate further these flow transitions. The cross-wire probe permits separation of the two dominant fluctuating velocities, giving two digitised data records suitable for further analysis by means of the cross-correlation function, the cross-spectrum and the phase spectrum. The basic concepts are given in currently available textbooks (eg Beauchamp and Yeun[2] and Jenkins and Watts[3]). The software was developed in the form of subroutines which were incorporated in the digital acquisition program documented elsewhere[4].

Apparatus

In essence, the apparatus, described in detail elsewhere[1], consisted of a vertical concentric annular gap 1820 mm long comprising a 69.85 mm radius stationary outer and a rotatable inner cylinder. Two interchangeable Tufnol inner cylinders of radius 66.4 mm and 55.9 mm respectively were used to provide narrow and wide gap configurations, of radius ratio 0.955 and 0.8. In this investigation, only the latter was employed. The working fluid was air which flowed down the annular gap; values of the axial Reynolds number were determined by means of orifice plates calibrated in accordance with BS1042. Measurements were made 1482 mm from the inlet, which was well within the region of fully developed flow.

* Project Engineer, Esso Production Malaysia Inc, Kuala Lumpur, Malaysia
† Senior Lecturer, Department of Mechanical Engineering, University of Leeds, Leeds UK, LS2 9JT
Received 16 September 1981 and accepted for publication on 26 February 1982

Cross-wire probe signals

The fluctuating tangential (u_t) and axial (u_a) velocity components can be separated by a cross-wire probe. It must be mentioned that, in the present experimental configuration, the probe is most sensitive to the radial velocity component due to its symmetry about the radial axis (Fig 1).

In the cylindrical coordinate system, the cross-probe can be positioned either along the r, a plane or the r, t plane. Ideally, the probe should be placed in the a, t plane, where it is most sensitive to components u_t and u_a. This was not possible, however, due to the limitations of the apparatus and, therefore, several assumptions had to be made, which will be discussed later. In this investigation, the probe was

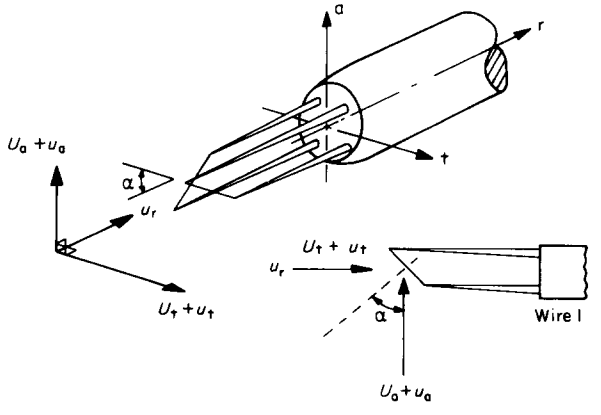

Fig 1 Position of X-probe, showing main components of velocity

placed as shown in Fig 1 and, radially, at mid-gap. The three-dimensional flow field experienced by the probe consists of U_a+u_a, U_t+u_t, and u_r in the axial, tangential and radial directions respectively.

Considering the first wire, the components of velocity can be resolved perpendicularly to the wire, where α is the angle between the vertical and the mean flow perpendicular to the wire. Simmers and Coney[5] showed that the radial velocity component was small compared with the mean axial and tangential velocities in spiral vortex flow. Therefore, since the present investigation is not concerned with the precise determination of u_t and u_a, the influence of the radial component $u_r \sin \alpha$ will be neglected.

Now, the mean effective velocity ($\bar{U}$) is given by:

$$\bar{U} = U_c + u_a \cos \alpha + u_t \tag{1}$$

where U_c is the velocity component normal to the wire. Also, King's Law gives:

$$V_2 = A + B\bar{U}^n \tag{2}$$

From Eqs (1) and (2) and with n = 0.45 for the probe:

$$V^2 = A + BU_c^{0.45}\left\{1 + 0.45\frac{u_a \cos \alpha}{U_c} + 0.45\frac{u_t}{U_c}\right\} \tag{3}$$

The relationship between the voltage fluctuation v and the velocity fluctuation is given by:

$$v \propto \frac{u_a \cos \alpha}{U_c} + \frac{u_t}{U_c} \tag{4}$$

The precise form is not essential since the constants can be determined by calibrating the probe. For the present purposes the signal from wire 1 in the position shown in Fig 1 will be of the form:

$$v_1 = C_1 u_t + C_2 u_a \cos \alpha \tag{5}$$

where constants C_1 and C_2 are approximately equal.

The second wire located near the first is identical except for the opposite inclination to the flow. The fluctuating signal output will be:

$$v_2 = C_1 u_t - C_2 u_a \cos \alpha \tag{6}$$

Combining Eqs (5) and (6), the velocity components u_t and u_a can be expressed in terms of the linearised voltage fluctuations v_1 and v_2 to give:

$$u_t = \frac{v_1 + v_2}{2C_1} \tag{7}$$

and

$$u_a = \frac{v_1 - v_2}{2C_2 \cos \alpha} \tag{8}$$

The constants C_1 and C_2 will be compensated for when the signal is linearised and $\alpha = 45°$. Hence, the components can be separated and the individual signals u_t and u_a analysed to find their statistical properties. The degree of relationship between the two signals can be determined by the cross-correlation function, the cross spectrum and the phase spectrum. A brief description of the method of computation of these quantities is given below.

Notation

A, B, C	Constants
b	Annular gap width ($R_2 - R_1$)
d_e	Equivalent diameter of annulus ($2b$)
E	Energy of data window
f	Frequency
I	Operator
$I(m)$	Imaginary part of a complex number
k	Index for data sequence
M	Number of samples
n	Constant
N	Annular radius ratio (R_1/R_2)
$P_x(f)$	Power spectral density function of signal $x(t)$
$P_y(f)$	Power spectral density function of signal $y(t)$
$P_{xy}(f)$	Cross spectral density function
R_1	Radius of inner cylinder
R_2	Radius of outer cylinder
$Re(\ )$	Real part of a complex number
$R_x(\tau)$	Autocorrelation function of signal $x(t)$
$R_y(\tau)$	Autocorrelation function of signal $y(t)$
$R_{xy}(\tau)$	Cross-correlation function of $x(t)$ and $y(t)$
Re_a	Axial Reynolds number $\left(\frac{U_m d_e}{\nu}\right)$
T	Digital time record ($M\Delta t$)
Ta	Taylor number $\left(\frac{2\Omega_1^2 R_1^2 b^3}{(R_1+R_2)\nu^2}\right.$ for a wide gap$\left.\right)$
u	Fluctuating velocity component
U	Mean velocity component
$\bar{U}$	Mean effective velocity (vector sum of axial and tangential velocity components)
v_1, v_2	Linearised fluctuating voltages (Eqs 5 and 6)
V	Mean voltage
$x(t)$	Continuous time signal
x_i	Discrete representation of signal $x(t)$
X_k	Discrete Fourier integral
X_k^*	Complex conjugate of X_k
$y(t)$	Continuous time signal
y_i	Discrete representation of signal $y(t)$
α	Angle
Δt	Sample interval
μ	Dynamic viscosity of fluid
ν	Kinematic viscosity of fluid (μ/ρ)
ρ	Density of fluid
τ	Time delay of correlation function
ϕ	Phase difference
ω	Frequency ($2\pi f$)
Ω_1	Inner cylinder angular velocity

Subscripts

a	Axial flow direction
r	Radial flow direction
t	Tangential flow direction

Cross-correlation function

The similarity between two signals $x(t)$ and $y(t)$ at any instant can be obtained by shifting the time axes relative to one another, the calculated mean product being repeated at various time delays. This is the principle of the cross-correlation function which, in its discrete form, may be expressed as:

$$R_{xy}(k\Delta t)=\frac{1}{M}\sum_{i=1}^{i=M} x_{i\Delta t}\cdot y_{i\Delta t}+k\Delta t \qquad (9)$$

where $k=1.2\ldots,K$, where K is the number of correlations required for a time delay of $\tau=K\Delta t$.

The importance of this function is that it contains information absent in the auto-correlation function, namely that concerning phase differences. For example, if two signals $x(t)=C_1\sin(\omega t+\phi)$ and $y(t)=C_2\sin(\omega t+\phi')$ are cross-related, the function will be:

$$R_{xy}(\tau)=$$

$$\lim_{T\to\infty}\frac{C_1C_2}{2T}\int_{-T}^{T}\sin(\omega t+\phi)\sin(\omega(t+\tau)+\phi')\,dt \qquad (10)$$

The expansion of Eq (10) using trigonometric identities will remove most of the terms, leaving

$$R_{xy}(\tau)=\frac{AB}{2}\cos(\omega\tau+\phi-\phi') \qquad (11)$$

Hence, the cross-correlation of two signals of similar frequencies will give the phase difference of the two signals. However, when higher frequency components are superimposed on a basic sinusoid, the function has limitations in that it will not give the phase difference. Nevertheless, the existence of correlation between the two signals is denoted by a sharp peak in the cross-correlogram plots for specific time displacements. The cross-correlation is normally presented in a dimensionless form defined as:

$$\bar{R}_{xy}(\tau)=\frac{R_{xy}(\tau)}{\{R_x(1).R_y(1)\}^{1/2}} \qquad (12)$$

Furthermore, as for the case of the auto-correlation function, a Fourier transform pair exists for the cross-correlation function and is termed the cross-spectral density function $P_{xy}(f)$.

Cross-spectrum and phase spectrum

Although the cross-correlation shows the degree of similarity between two signals, it gives no information about the relative phase characteristics of the two signals. In order to detect this similarity, and at the same time identify the phase, the cross-spectrum is used.

The generalised form of the cross-spectrum analysis involves the fast Fourier transforms of the two signals $x(t)$ and $y(t)$ giving $X(f)$ and $Y(f)$ respectively. Analogous to the computational procedure for the power spectrum, the raw spectral estimates are given by:

$$P_{xy}(k)=2(X_k^*Y_k) \qquad (13)$$

where X_k^* is the complex conjugate of the discrete transform X_k. The function is expressed in the frequency domain as:

$$P_{xy}(f)=\frac{P_{xy}(k).k}{EM\Delta t}\text{ where } k=1,2\ldots,M/2 \qquad (14)$$

The cross-spectrum $P_{xy}(f)$ will show how closely $X^*(f)$ and $Y(f)$ are related over the frequency range of interest.

If $X(f)$ and $Y(f)$ are complex, $P_{xy}(f)$ will have a real and imaginary part. Since $|P_{xy}(f)|$ increases with the increase in values of the real and imaginary parts, a relation between $|X(f)|$ and $|Y(f)|$ can be derived. The real and imaginary parts of $P_{xy}(f)$ can be related by the phase spectrum $\phi_{xy}(f)$ given by:

$$\phi_{xy}(f)=\frac{180}{\pi}\arctan\frac{Im(P_{xy})}{Re(P_{xy})} \qquad (15)$$

where $\phi_{xy}(f)$ is in degrees.

Hence the magnitude and phase characteristics in the signals can be determined by these spectra. Subroutines for the computation of these quantities were written for easy implementation into the main data acquisition program, given elsewhere[4].

Experimental procedure

A DISA 55P61 cross-wire probe was used, having a separation distance of 0.4 mm between the two sensors, and was connected to two DISA 55M01 anemometer main units and low pass filter units. The hot wire signals were amplified by a non-inverting amplifier and connected to two channels of an analogue to digital converter (adc). Since the phase characteristics between the signals are very important in the present determination, both channels were sampled simultaneously by switching on the parallel sample and hold amplifiers on the adc. The experimental arrangement for this investigation is shown in Fig 2. Clipping levels were avoided by displaying the pre-amplified and amplified signals on the oscilloscope.

The sampled signal is stored in an integer array $IX(I)$, $I=1,2,\ldots,M$, where the odd array elements, ie $IX(1)$, $IX(3)$, etc, represent the signal from the first wire and the even array elements, ie $IX(2)$, $IX(4)$, etc., that from the second wire. Once sampled, the separation of these two signals can be easily performed on the computer. Results were taken at $Re_a=500$ for a range of inner cylinder rotational speeds. The number of samples was 2^{13} for two channels with $\Delta t=5$ ms. The signals obtained

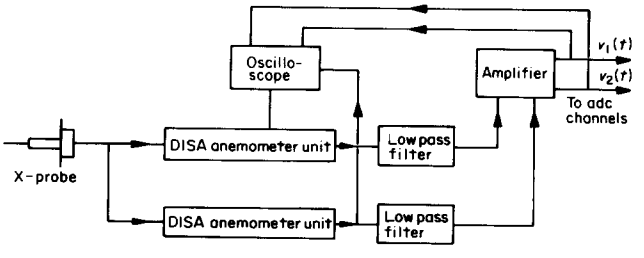

Fig 2 Experimental arrangements used with X-probe

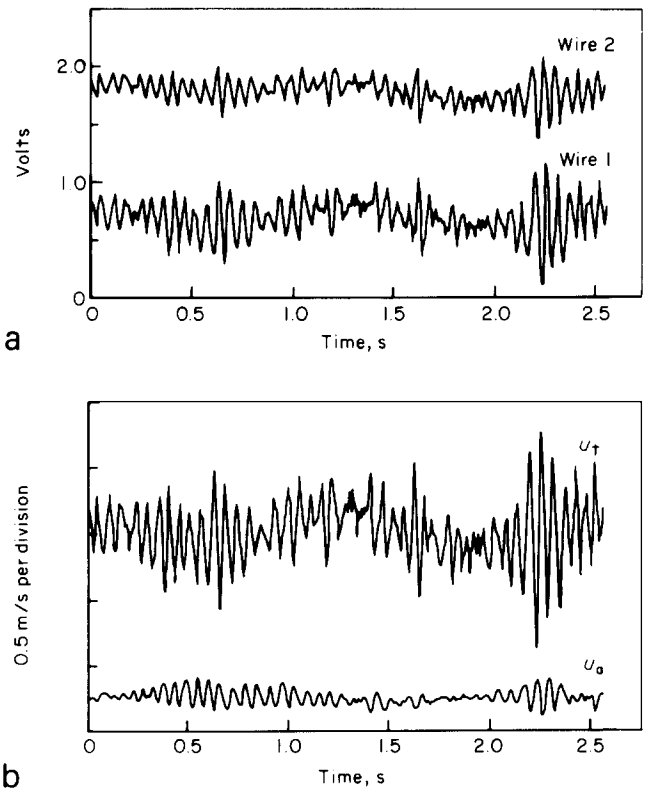

Fig 3 X-probe signals and fluctuating velocity components for $\mathrm{Re_a} = 500$, $\mathrm{Ta} = 10\,620$

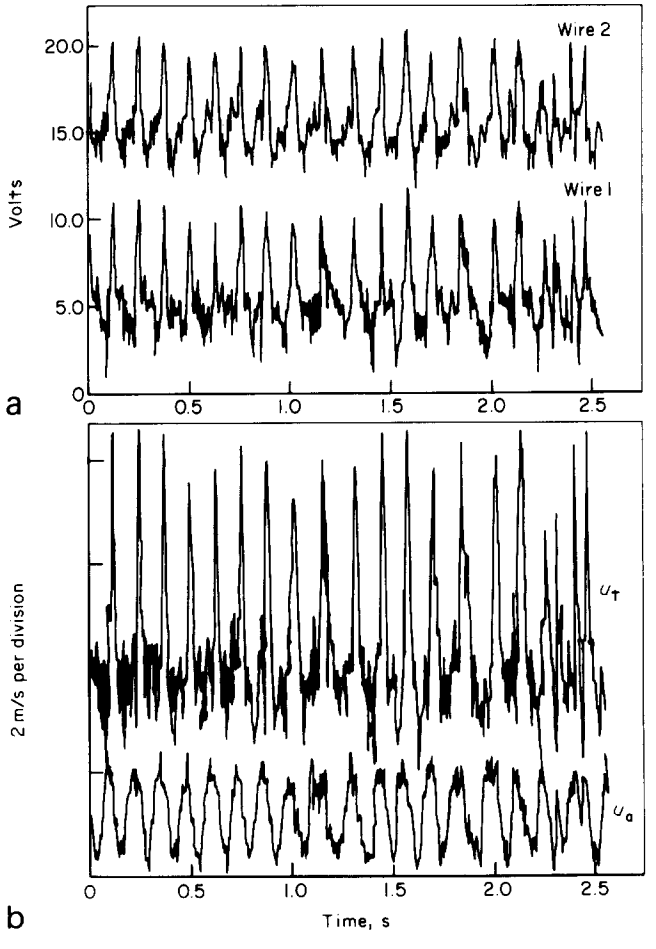

Fig 4 X-probe signals and flutuating velocity components for $\mathrm{Re_a} = 500$, $\mathrm{Ta} = 5.27 \times 10^6$

from the two wires can be seen in Fig 3(a) at the onset of the spiral vortex instability. The linearisation of the two signals was performed on the computer, the probe having been calibrated on the DISA 55D90 calibration apparatus. After linearisation, the mean velocities were removed and the linearised signals combined to give u_t and u_a.

The separated velocity components are shown in Fig 3(b), where the tangential velocity component is seen to be much higher than the axial component, indicating a greater concentration of vortex energy in that direction. With the increase in speed, the signals from both wires begin to be 'peaky' at $Ta = 5.27 \times 10^6$, as shown in Fig 4(a). In Fig 4(b), the component u_t increases markedly, giving an indication of the high rates of shear in that direction. The axial component u_a tends to be more uniform with higher harmonics being apparent at the peaks.

Results and Discussion

The results of Fig 5(a) show the flow condition at criticality, where the individual power spectrum of u_t is given by $P_x(f)$ and that for u_a by $P_y(f)$. The cross-spectrum of u_t and u_a is $P_{xy}(f)$ and the phase spectrum is $\phi_{xy}(f)$. The tangential spectrum is seen to have the highest magnitude with a dominant peak frequency of 0.8 Hz and a frequency band spread over 11 to 24 Hz. The axial frequency spectrum $P_y(f)$ shows the dominant frequency occurring approximately at this band of frequencies, suggesting that this is due to the axial flow component. It is also clear that the tangential peak is present in the axial spectrum, but is suppressed. Turning to the cross-spectrum results, the dominant frequencies in the flow are due to the combined effects of u_t and u_a, the former being greater. Comparing the spectra of $P_x(f)$ and $P_y(f)$, it can be seen that in the spiral vortex instability there is a large degree of similarity between the axial and tangential directions. The phase spectra $\phi_{xy}(f)$ give the relative phase differences occurring over the range of frequencies displayed. A sharp peak in the phase spectrum indicates that, at the particular frequency where the peak occurs, the components u_t and u_a are either positively or negatively out of phase by a value corresponding to that of the peak. If they are perfectly in phase, then $\phi_{xy}(f) = 0$. Referring again to the phase spectrum in Fig 5(a), the phase difference is normally small where the dominant peaks occur, eg in the frequency band 16–20 Hz.

The auto-correlograms for u_t (or $R_x(\tau)$) and u_a (or $R_y(\tau)$) and the cross-correlograms for u_t and u_a (or $R_{xy}(\tau)$) are given in Fig 5(b), from which it can be seen that the periodicity in the auto-correlograms is clearly distinguishable in the axial and tangential directions. The periodic cross-correlogram for $R_{xy}(\tau)$ shows a high degree of regularity and has a periodicity very similar to that for $R_x(\tau)$ and $R_y(\tau)$. The positive peak value of the function shows that u_t and u_a are in phase, except for the observable time delay. These findings are in good agreement with other investigations at the critical Taylor number[7,8].

The spectral results for the chaotic mode at $Ta = 514\,400$ are shown in Fig 6(a). In this regime,

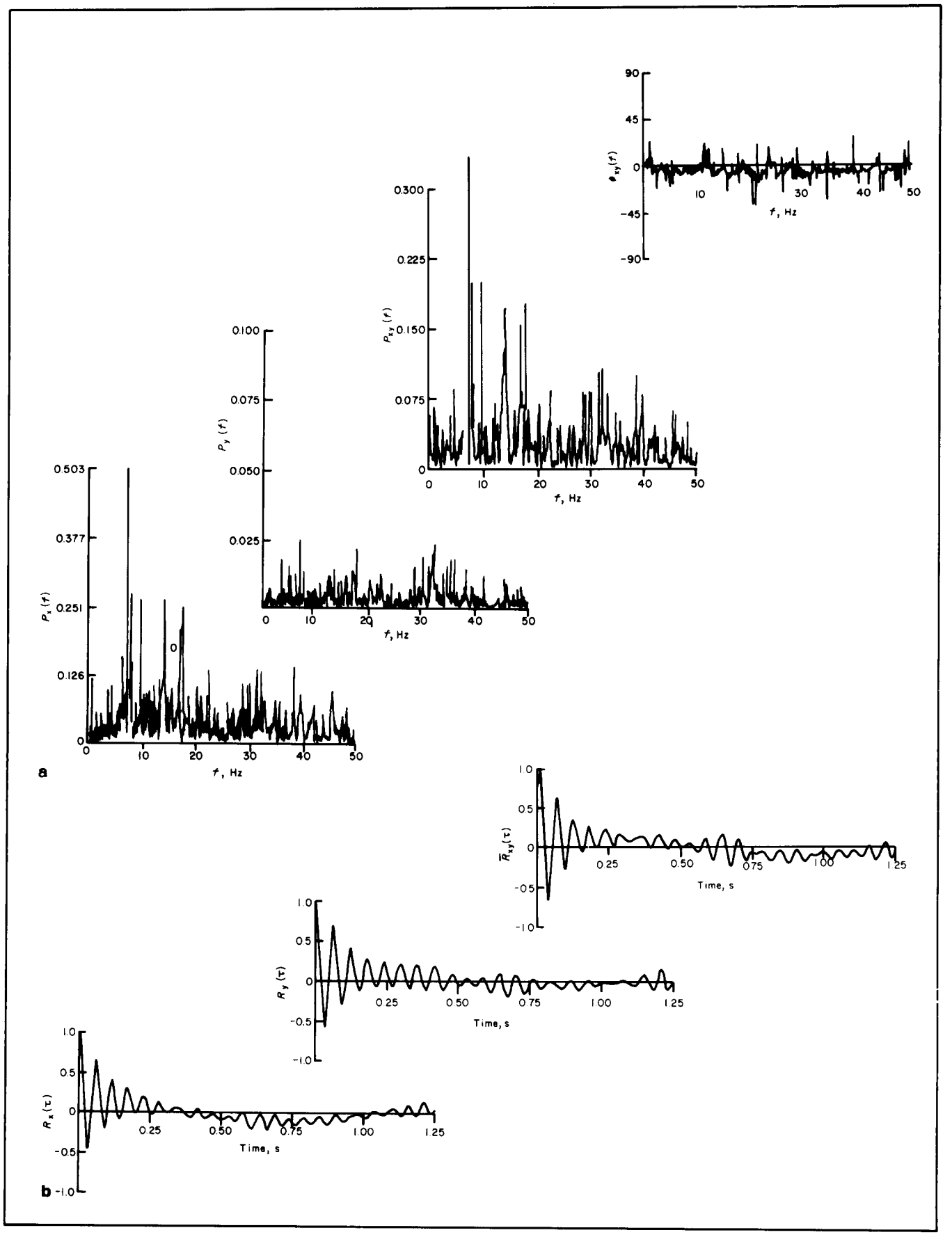

Fig 5 (a) Cross spectrum and phase spectrum (b) Auto- and cross-correlogram (Ta = *10 620*, N = *0.8*, Re_a = *500)*

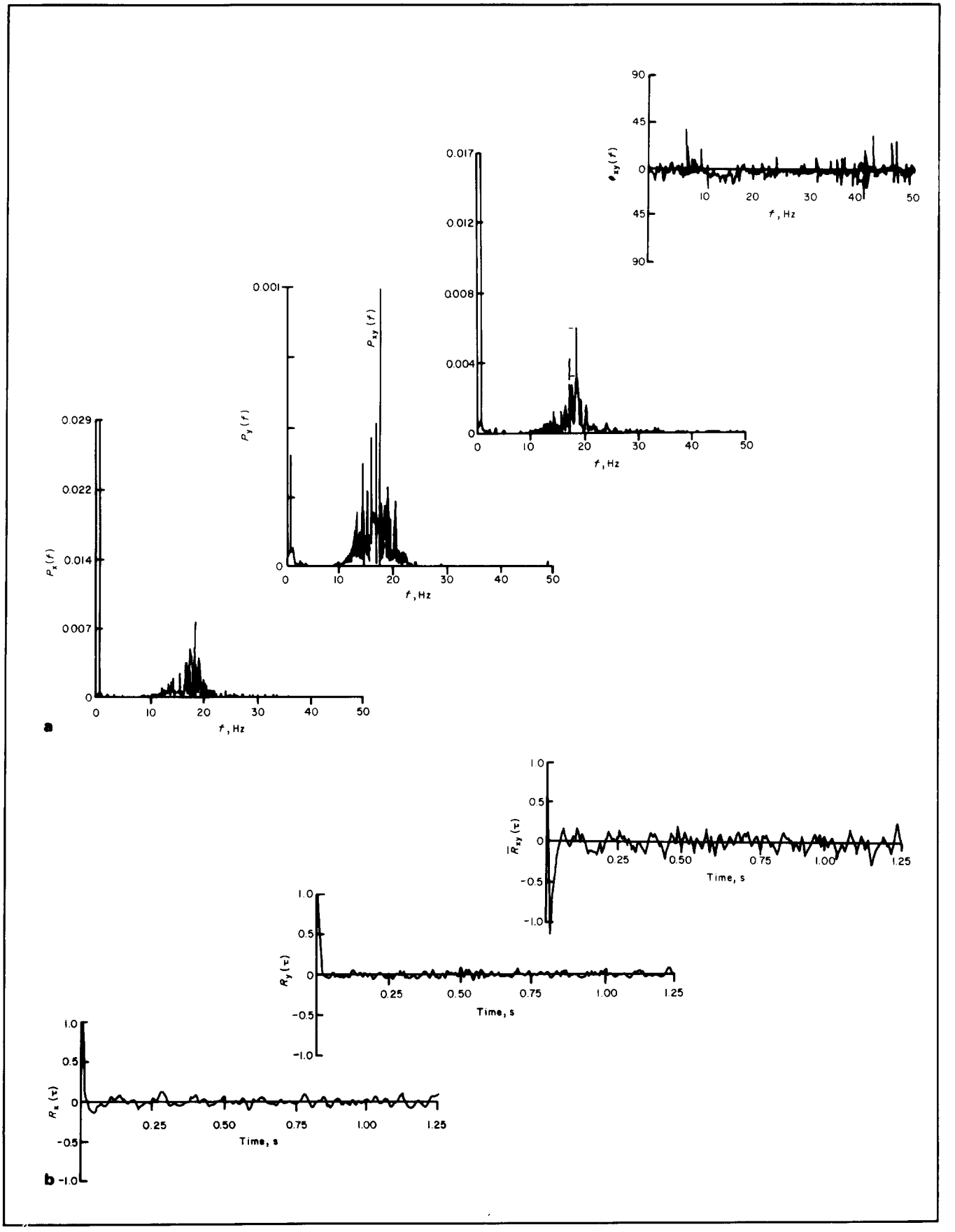

Fig 6 (a) Cross spectrum and phase spectrum (b) Auto- and cross-correlogram (Ta = *514,400)*

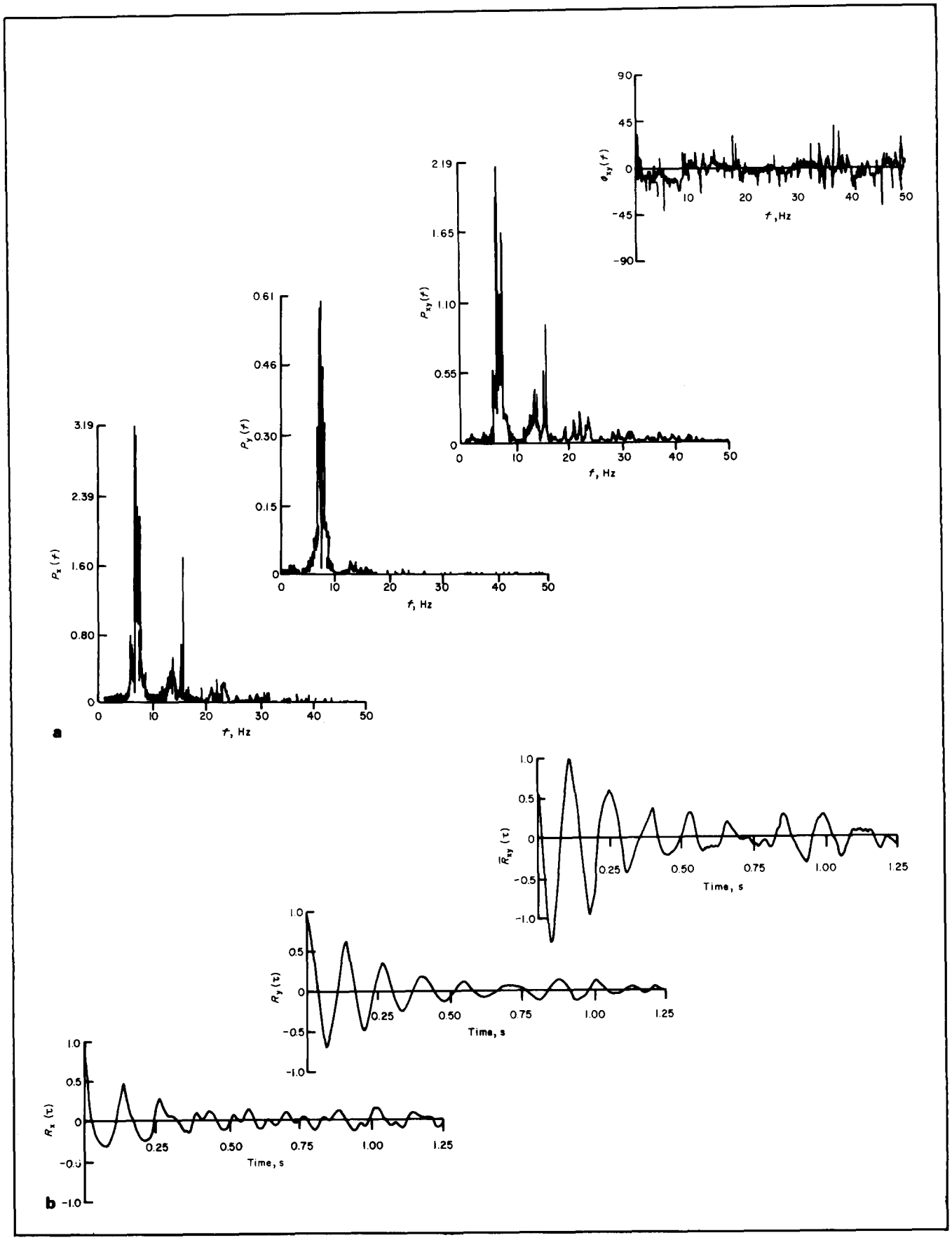

Fig 7 (a) Cross spectrum and phase spectrum (b) Auto- and cross-correlogram (Ta $= 5.27 \times 10^6$)

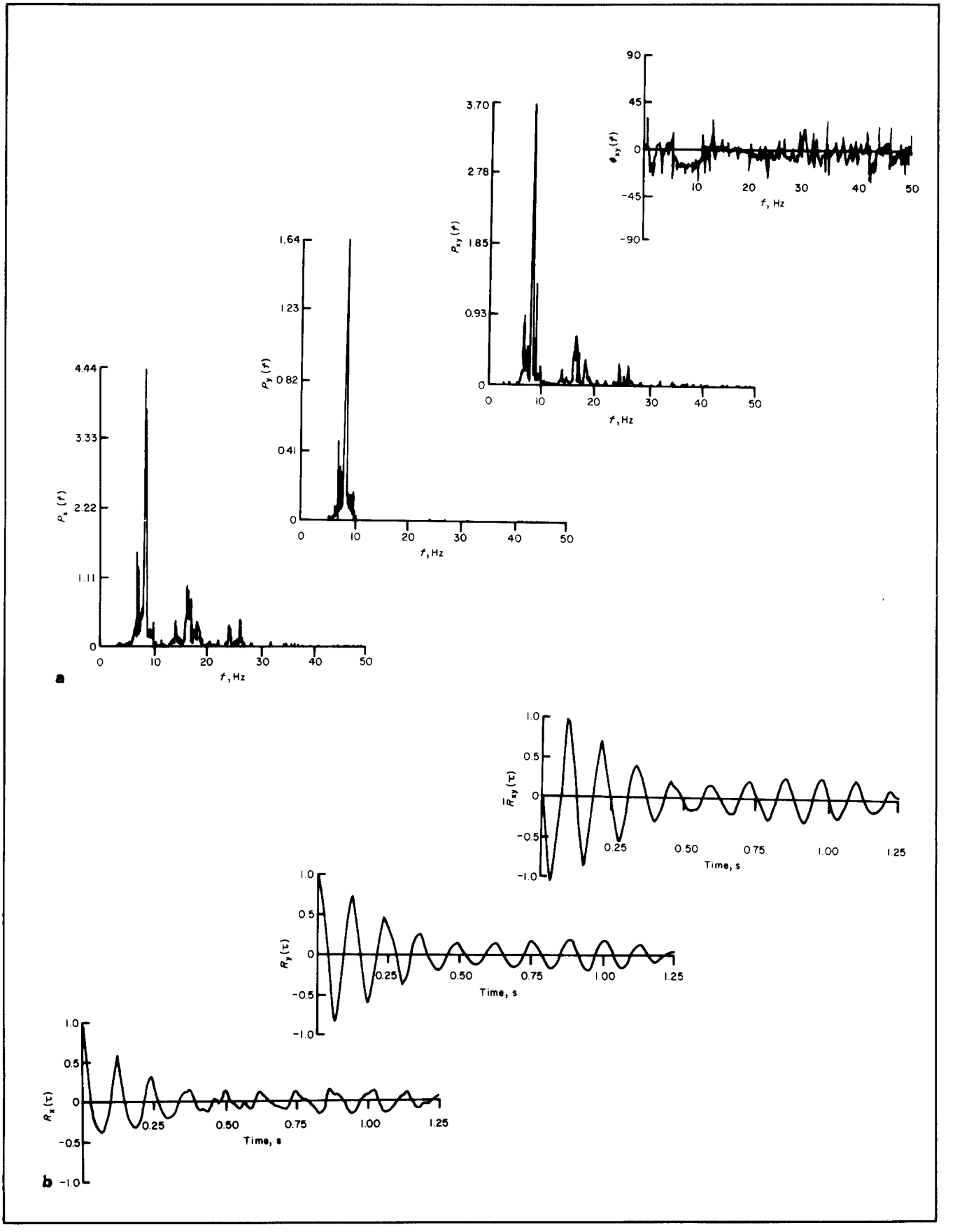

Fig 8 (a) Cross spectrum and phase spectrum (b) Auto- and cross-correlogram (Ta = 12.2×10^6)

the multi-frequency spectrum for P_x and P_y contains several dominant frequency peaks, the cross-spectrum P_{xy} being useful in delineating the frequencies common to both the axial and tangential spectra. A dominant frequency peak at 7 Hz in the cross-spectrum is seen to appear in both the P_x and P_y spectra. It may be seen that the phase spectrum is beginning to show negative phase differences for bands of frequencies that are similar axially and tangentially. This shows that, although the vortex flow is fundamentally the same in both directions, the variation in the axial and tangential phases are different, as would be expected at the onset of the wavy mode in the azimuthal direction. The correlograms in Fig 6(b) illustrate the complexity of the flow with a sharp negative peak in the cross-correlogram, indicating that the velocities are still related but there is a phase change present.

Moving into the turbulent vortex regime, the strongly periodic flow, represented by the broad spectral peaks with several harmonics, can be seen in Fig 7(a). It is noticeable that the frequency band of the dominant broad spectral peak again displays a negative phase difference of 15° in two directions, whereas the higher frequencies are approximately in phase. This re-emergence to a periodic flow can be observed in the correlograms of Fig 7(b), the axial direction containing greater periodicity. At $Ta = 12.2 \times 10^6$, (Fig 8(a)), the side frequencies disappear, and a single dominant peak spectrum begins to emerge. The axial spectrum P_y shows the high magnitude of this turbulent vortex mode compared with the other harmonics of the flow in the axial direction. This provides further evidence to support the heat transfer results by Wan and Coney[6], where the axial flow component is found to be insignificant in influencing the turbulent vortex mode over a similar flow range. The phase spectrum in Fig 8(a) gives a larger phase difference at the dominant frequency compared with the previous flow condition in Fig 7(a). Hence, it appears that, as the tangential velocity gradient increases, the turbulent vortex mode begins to show a greater phase change relative to the axial and tangential directions. The correlograms of Fig 8(b) show an increased periodicity as the turbulent vortex mode becomes more established, with the axial component being more periodic than the tangential component. The phase change is also evident from the cross-correlogram, with the first peak value being negative.

Burkhalter and Koschmieder[9], in their studies of super-critical Taylor vortex flow without axial flow, measured the size (termed by them the 'wavelength') of the vortices using a cathetometer. They observed that, at very high Taylor numbers, the wavelength of the vortices increased over that at criticality. No conclusions were drawn regarding the nature of the flow and they termed it as either 'doubly periodic or truly turbulent'. It is believed that the present results provide an insight into this phenomenon.

Comparing the auto-correlograms and cross-correlograms for the evolution of the flow, it appears that the spiral vortices at the critical Taylor number are smaller than the turbulent vortices. This is confirmed by a later cross-over point in the correlograms for turbulent vortex flow, even though the mean flow velocities are extremely high. Also their occurrence at low frequencies suggests that they are large vortices. However, the present results only provide a qualitative view of this occurrence, owing to the lack of a length factor. Nevertheless, this problem can be overcome by having two X-probes separated by a distance which is less than the gap width, the cross-correlation function giving the time required for the turbulent vortices to pass the two probes axially or tangentially. Also, the drift velocity of the vortices in both directions can be determined.

Conclusions

The use of the cross-wire probe as a preliminary to more complex digital analysis has further substantiated earlier results and has also given additional information regarding the flow at $Re_a = 500$. It is clear now that the spiral vortex flow remains basically unchanged in the axial and tangential directions, with increase in Taylor number, oscillating in phase in the two directions. It was noted, however, that with increasing Taylor number, the chaotic and turbulent vortex modes render a steadily increasing negative phase difference between the tangential and axial velocity fluctuations. A gradual dominance of the tangential velocity gradient was observed and, in the turbulent vortex mode, the axial velocity gradient became small. The cross-wire probe provides further means for the improvement of the digital techniques; it is hoped that it will be further used by the authors as well as by others to add to the growing knowledge of spiral vortex flow transitions.

References

1. **Wan C. C. and Coney J. E. R.** Transition modes in adiabatic spiral vortex flow in narrow and wide annular gaps. *Int. J. Heat & Fluid Flow, 1980, 2(3), 131–138*
2. **Beauchamp K. G. and Yuen C. K.** Digital methods for signal analysis. *George Allen and Unwin, London, 1979*
3. **Jenkins G. M. and Watts D. G.** Spectral analysis and its applications. *Holden-Day Inc., San Francisco, 1968*
4. **Wan C. C.** A study of adiabatic and diabatic spiral vortex flow transitions between concentric cylinders using digital techniques. *Ph.D. thesis, Leeds University, 1980*
5. **Simmers D. A. and Coney, J. E. R.** Velocity distributions in Taylor vortex flow with imposed laminar axial flow and isothermal surface heat transfer. *Int. J. Heat & Fluid Flow,* 1980, *2(2), 85–91*
6. **Wan C. C. and Coney J. E. R.** An experimental study of diabatic spiral vortex flow. *Int. J. Heat & Fluid Flow,* 1982, *3(1), 31–38*
7. **Donnelly R. J. and Fultz D.** Experiments on the stability of spiral vortex flow between rotating cylinders. *Proc. N.A.S. Physics, 1960,* **46**, *1150–1154*
8. **Snyder H. A.** Experiments on the stability of spiral flow at low axial Reynolds numbers. *Proc. Roy. Soc., 1965,* **A.265**, *198–214*
9. **Burkhalter J. E. and Koschmieder E. L.** Study of supercritical Taylor vortex flow. *J. Fluid Mech., 1973,* **58**, *pt. 3, 547–560*